I R A M P
5(2), July-Dec. 2014, pp. 73-81

ISSN: 2229-3159

Empirical Formulae for Electron Density Diagnostics from H_α and H_β Line Profiles

DAVID M. SURMICK AND CHRISTIAN G. PARIGGER

Center for Laser Applications
University of Tennessee Space Institute
411 B.H. Goethert Parkway
Tullahoma, TN 37388

ABSTRACT: We present empirical formulae for the electron density vs. line profile widths and shifts developed from precise measurements of hydrogen Balmer series alpha and beta emissions for diagnostics of laser-induced plasma. The formulae are for the Stark width and Stark red shift of the H_α line, as well as for the Stark width and peak separation of the H_β line and are tested using measurements of H_α and H_β emissions in laser-induced plasma following ablation of an aluminum surface in a hydrogen gas atmosphere. The H_α and H_β line widths and H_α line shift are determined by fitting the measured spectra with Voigt profiles. The H_β peak separation is found by direct inspection. For example, the H_β line shows N_e of $3.2\pm0.3\times10^{17}$ cm^{-3} and $3.8\pm0.5\times10^{17}$ cm^{-3} from the line width and peak separation, respectively, at a time delay of 0.65 μs from plasma generation.

PACS Codes: 52.38.Mf, 32.70.Jz, 33.70.Jg

KEY WORDS: Laser Ablation, Line Shapes, Hydrogen, Aluminum, Laser-Induced Breakdown Spectroscopy

1. INTRODUCTION

Laser-induced plasma is a rich physical environment with many complex, dynamical processes occurring, including impact processes of charged particles and the associated fluid physics of a rapidly expanding gas or plasma. As well, the applications of laser-induced plasma, particularly in the laser ablation of solid targets, is wide spread and varied, which includes assembly line diagnostics of metal alloys, sorting of scrap metals, and more fundamental studies of laser material interactions and rapid shock wave propagations [1, 2, 3, 4, 5]. In the ablation of a target sample with nominal nanosecond pulsed radiation, a portion of the target material and surrounding atmosphere is vaporized and mixes together. Subsequently, ionization occurs as a hot, dense plasma is formed through electron impact and multi-photon ionization processes [6, 7]. In terms of diagnostics for both applied and fundamental studies, the prime parameters of interest are the electron density, N_e, and the temperature. Investigations of the spectral line shape allow for the spectroscopic probing of the plasma. The collisional broadening of charged and neutral species in the plasma allow one to infer the N_e from the total Stark profile of a spectroscopic emission and the temperature may be found from several observed ionic and/or atomic emissions through use of the Boltzmann and Saha-Boltzman relations.

Following the plasma initiation from optically-induced breakdown, the plasma will begin to decay after a short (~ 20 ns) period of expansion. In the case of nanosecond pulsed laser ablation, the plasma is further pumped as the plasma is already formed while laser radiation is still incident on the target sample and thus increases the amount of free elections [8]. Further, when ablating a solid target sample (aluminum, titanium, steel alloys, *etc.*), the availability of solid state electron densities (~10^{22} cm^{-3}) further increases the electron density in the plasma and

therefore the collisional broadening of spectroscopic emissions is increased. The wide spread availability of sensitive spectroscopic equipment with sufficient temporal and spatial resolution allow one to spectrally probe the earliest times of the plasma decay following laser ablation. An excellent candidate for diagnostics of such laser-induced plasma is the hydrogen Balmer series due to its extensive history of theoretical, numerical, and experimental studies in laser plasma [9, 10, 11, 12], as well as the prevalence of sensitive spectroscopic equipment in the nominal visual section of the electromagnetic spectrum. Additionally, these lines are reasonably isolated from interfering spectral emissions in nominal air spark experiments.

In this work, we consider the use of empirically developed formulae that relate the H_α Stark width and Stark red shift and the H_β Stark width and peak separation for laser-induced plasma diagnostics in the early plasma time evolution. While there are already similar formulations for the line width parameters in terms of the N_e [13, 14, 15], a formulation that is applicable for the high electron densities encountered in laser ablation plasma is desired. This is accomplished as the data used to produce our formulae were analyzed using the formalism of the convergent theory of Oks [16, 17, 18]. The presented formulae are subsequently applied to the H_α and H_β spectra observed following laser ablation of an aluminum target sample with nanosecond pulsed laser radiation and are compared to similarly available formulae from the literature.

2. EMPIRICAL FORMULAE

The line shape of a spectral emission in laser-induced–plasma is subject to significant Stark broadening due to the strong local micro-fields in the ionized plasma. While helpful, simulations of Stark broadened emissions are cumbersome and complex to calculate [19]. While it is the line shape that contains all the underlying physics of laser plasma, it is customary for use in experimental studies to only extract the line width (FHWM) in an attempt to find the electron density, typically by fitting a Lorentzian profile to experimental data. Under the influence of Stark broadening mechanisms, the line width is known to be proportional to some power of N_e, with the power being less than one [13]. This has been shown extensively in the first semi-classical approaches to solve the broadening of spectral lines from collisions in plasma from charged particles from the 1960's onward [13, 20, 21]. Further additions were made to this theory, however, as was customary, tables of Stark widths and electron densities grew, rather than the development of experimental formulae. This work serves to move from the Stark tables to empirically driven formulae that relate the electron density with line width and shift parameters of measured spectral line profiles.

We consider the alpha and beta line emissions of the hydrogen Balmer series. The empirical formulae for the H_α and H_β line shape plasma diagnostics are developed from precisely collected Balmer series data by Parigger *et al.* [22] that were subsequently analyzed using the convergent theory of Oks [16, 17, 18]. The prime advancements from the previous, semi-classical approaches that use micro-field interactions in the so-called quasistatic approximation are indirect coupling of electron and ion broadening principles and accelerations of the electron due to the ion field, in addition to an improved treatment of the plasma ion dynamics.

As is the case with many other experimental and theoretical treatments of Stark broadening, tables of line widths and their associated N_e and temperature are the standard. To develop the empirical formulae here, we use exclusively the Stark tables of line widths and N_e from Refs. [16] and [22] which treat the electron density determination using the theory Oks. We note that Tables 9.7-9.9 in Ref. [16] are identical to Tables 2-4 in Ref. [22].Data from Tables 3 and 4 from Ref. [22] were used to develop the N_e vs. FWHM (Δw) and N_e vs. red shift ($\Delta\delta$)formulae for the H_α line widths and red shifts, respectively. Fits were performed in Log-Log linear space. The results of these fits for the H_α line are displayed in Figure 1. The fits were obtained using a nominal linear least squares fitting method.

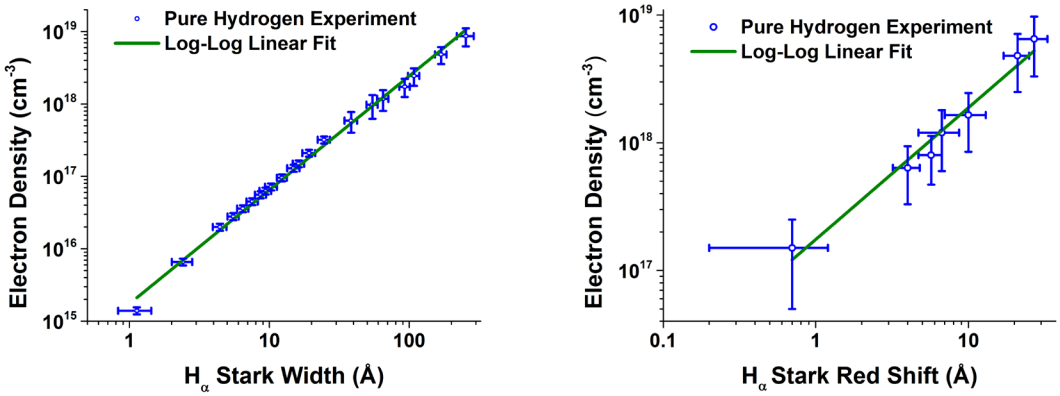

Figure 1: Linear Log-Log fits used to develop the H_α line width and line shift formulae

The error bars for the data points represent the indicated errors in the line widths and shifts in addition to the accuracy of the given line parameter diagnostic. For the H_α line this accuracy amounts to approximately 20 percent. Adjusted R^2 values are used to measure the goodness of fit in each fitting case and for the H_α line width and red shift are found to be 0.9951 and 0.9878, respectively. The resulting formulae for the FWHM and shift are displayed below in Equations 1 and 2. They have been algebraically manipulated from their original Log-Log state to show a power law formulation, in similar fashion to other recent works [14, 15, 23].*

$$\Delta w_{H_\alpha}[nm] = 1.31\left(\frac{N_e[cm^{-3}]}{10^{17}}\right)^{0.64\pm0.03} \quad (1)$$

$$\Delta \delta_{H_\alpha}[nm] = 0.055\left(\frac{N_e[cm^{-3}]}{10^{17}}\right)^{0.97\pm0.03} \quad (2)$$

The H_β line width and peak separation formulae were developed using Tables 2 and 1 from Ref. [22], respectively. Due to the double peak structure of the H_β line under the influence of Stark broadening, it is very difficult to determine the line shift; however, the separation of the H_β double peak structure is known to be dependent on the electron density [24, 25]. The peak separation N_e data used from Ref. [22] were calculated by correlating the magnitude of the peak separation with an H_β FWHM. Figure 2 shows the Log-Log linear fitting results of H_β line width (Δw) and peak separation ($\Delta\lambda_{ps}$).

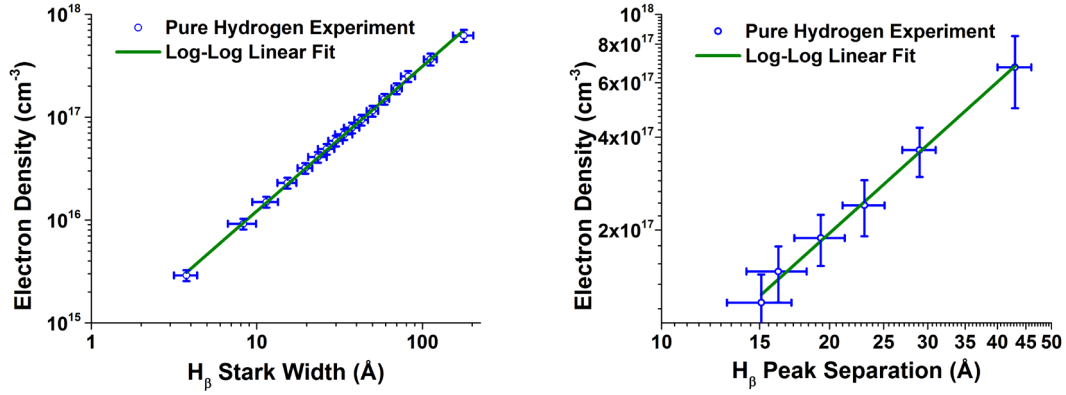

Figure 2: Linear Log-Log fits used to develop the H_β line width and peak separation formulae

For the line widths, the error bars in Fig. 2 are found in a similar manner to the H_α line widths and shifts, using the known accuracy of the H_β line width diagnostic of 5 percent. The error bars for the peak separation were found by carrying out the standard error propagation using the reported error bars in Table 1 of Ref. [22]. The resulting power law formulae for the FWHM and peak separation are displayed in Equations 3 and 4, respectively. The adjusted R^2 goodness of fit measures for the H_β FWHM and peak separation are 0.9996 and 0.9978, respectively.

$$\Delta w_{H_\beta}[nm] = 4.50\left(\frac{N_e[cm^{-3}]}{10^{17}}\right)^{0.71\pm0.03} \tag{3}$$

$$\Delta \lambda_{ps}[nm] = 1.32\left(\frac{N_e[cm^{-3}]}{10^{17}}\right)^{0.61\pm0.03} \tag{4}$$

Finally, we comment on the useful ranges of the determined formulae. For large N_e, the H_β line is very broad and its line width is difficult to distinguish from a free-free or free-bound measured continuum radiation, particularly for laser-induced plasma experiments at early plasma decay times. For the H_α line, its width becomes increasingly narrower for decreasing electron densities and is difficult to evaluate within experimental error margins below 10^{16} cm^{-3}. Figures 1 and 2 show a scope of several orders of magnitude(10^{15}-10^{19} cm^{-3}) in the range of the N_e determination for both the H_α and H_β line widths. For practical purposes it is most useful and less error prone for the H_β line width diagnostic to be used for N_e ranging from 10^{15} up to and approaching an upper limit of 10^{18} cm^{-3}. For investigations with larger expected N_e, greater than 10^{18} and up to 10^{19} cm^{-3}, H_α line shape diagnostics are suggested. The H_β peak separation has a limited scope of usability due to the asymmetric nature of the H_β double peak, as well as having line width and temperature dependencies for large N_e and its disappearance for low N_e; thus, the peak separation diagnostic is most useful in the N_e range near 10^{17} cm^{-3} and up to at most 10^{18} cm^{-3}.For the H_α line shift, it is in general difficult to determine for small shifts measured experimentally due to the physical limitations of most experimental apparati. This diagnostic is likely to be the most error prone due to this limitation and is best used at larger expected N_e values.

3. EXPERIMENTAL DETAILS

The laser ablation event is studied using spatially and temporally resolved spectroscopy methods. Here we consider laser ablation of an aluminum alloy 6061 target sample using a similar apparatus to previous Al laser ablation studies [1, 26]. The optical breakdown was initiated using a 14 ns pulsed, Q-switched Nd:YAG laser operating at it fundamental mode and at its fundamental frequency. The laser operated at a repetition rate of 10 Hz. The average energy per pulse was 120 mJ, resulting in a peak irradiance of approximately 30 GW/cm^2. Spectra are dispersed using a 0.64 meter Jobin-Yvon HR640 Czerny Turner style spectrometer installed with a 1200 grooves/mm grating. A two dimensional, time gated ICCD (And or iStar) is used to record the plasma emissions with spatial resolution. The overall time resolution possible was 6 ns and the overall spatial resolution used was 0.1 mm. The overall spectral resolution of the system was determined to be 0.15 nm. The temporal resolution was achieved by synchronizing the ICCD with the laser Q-switch. Each recorded spectrum represents an average of 100 laser ablation events to mitigate the shot to shot effects and variances that commonly occur in laser-induced breakdown experiments. Using so many laser shots does increase the possibility of sample matrix effects due to the shape and extent of the crater formed. These are to be considered minimal in the scope of 1 vs. 100 laser shots since we use a nanosecond pulsed laser system at a pressure near atmosphere, where more mass is ablated for smaller pulse widths and significantly reduced (< 100 Torr) pressures [27].

Optical breakdown was initiated in a gas cell containing 90 percent hydrogen with a 10 percent nitrogen buffer gas atmosphere at a pressure of 830 Torr, *i.e.* close to atmospheric pressure. Ultra-high purity nitrogen and hydrogen gas (99.999 percent pure) were used to fill the chamber. The correct mixtures were obtained using partial pressure addition of the hydrogen and nitrogen gas amounts. The gas cell was cleaned and evacuated using a mechanical/

diffusion pump apparatus prior to experimentation. The H_α spectra were chosen to be viewed at 0.15 and 0.4 μs time delays to show a temporal N_e gradient and display the use of empirical formulae for various N_e. The H_β spectra were viewed at a 0.65 μs time delay due to its significantly broader nature than the H_α line for similar N_e. This time delay also allows for simultaneous determination of N_e from the H_β peak separation. The times were also chosen, in part, to avoid line distortion effects from self-absorption, which is likely to occur for N_e greater than 2×10^{18} cm^{-3} [28].The gate width for all the measurements was 20 ns. The spectra were calibrated for the apparatus sensitivity response using a Halogen/Deuterium lamp with a constant temperature output. The apparatus wavelength response was calibrated using a gas discharge hydrogen lamp. Both calibrations were carried out prior to analysis.

4. RESULTS AND DISCUSSION

The electron density from the empirical formulae shown in Section 2 require that the line FWHM, shift, and/or peak separation be determined from the experimental data. While it is possible to determine these values using inspection methods, it is customary to fit the measured line profiles, particularly for the extraction of the line width. We consider the use of a Voigt profile for the H_α and H_β FWHM and the H_α Stark red shift determinations. For the H_β peak separation, we consider direct inspection of the measured line profile following data filtering to reduce the uncertainty of the H_β double peak positions due to noise effects. The Voigt profile is the convolution of Lorentzian and Gaussian line shapes. For a given experimental apparatus one may determine the so-called instrument function from wavelength calibration measurements and assign this width to a Gaussian function. Doing so allows for deconvolution of the measured line profile to its Lorentzian width which is then typically taken to describe the Stark broadened component of the line.

The instrument width is determined while performing the wavelength calibration with a hydrogen gas discharge lamp and is found be 0.15 nm on average throughout the spectral range of the Balmer series. The Voigt fitting is completed using a nonlinear least squares fitting routine, where the Voigt profile is tabulated using the Algorithm 916 method [29], with the Lorentzian width and line shift as fit parameters, in addition to the line amplitude and a linear offset. Figure 3 shows an ICCD image of measured H_β spectra at 0.65 μs time delay following optical breakdown and a sample Voigt profile fit used to extract the H_β FWHM. The fit represents a slit height of 6.1 mm. The inferred line width is 10.3±0.5 nm. Also shown in the right image of Figure 3 is a filtered line profile, which was used to reduce the noise on the line peak so that a more accurate peak separation is determined. We chose to use a 51 point Savitzky-Golay filter for this application. The determined peak separation was 3.0±0.6 nm. Using Equations 1 and 2, the electron density is found to be $3.2\pm0.3\times10^{17}$ cm^{-3} and $3.8\pm0.5\times10^{17}$ cm^{-3} for the H_β line width and peak separation, respectively. These inferred values show self-consistency when the error margin is considered. Despite using the filtered experimental data for the peak separation determination, the N_e result still shows a larger variability in the inferred value.

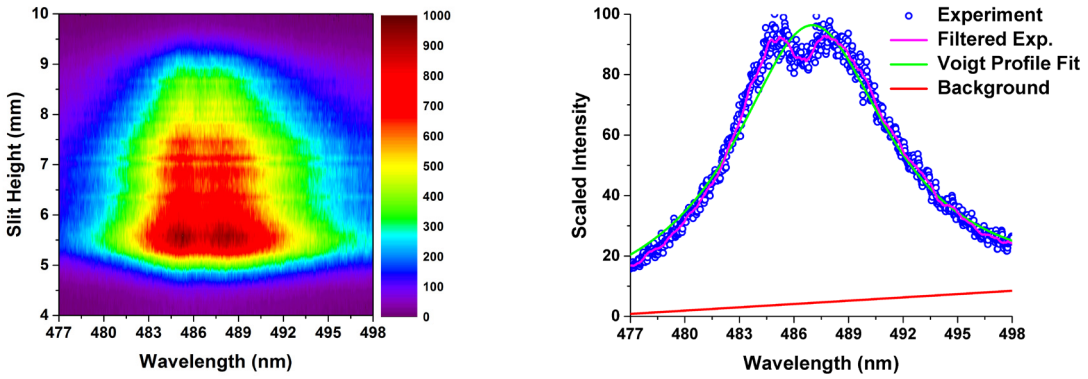

Figure 3: Two dimensional image of H_β spectra at 0.65μs time delay (Left) and Voigt profile fit to an H_β spectrum at a slit height of 6.1 mm used to extract the FWHM, as well as Savitzky-Golay filtered data used for the peak separation (Right)

Voigt profile fitting is also utilized to find the electron density from the H_α line width and shift. Figures 4 and 5 depict the spatial variation of the measured H_α spectra through ICCD images, as well as sample Voigt profile fits at 0.15 and 0.4 μs time delays following optical breakdown, respectively. The fits in both Figures 4 and 5 are performed at the same 6.1 mm slit height as the fitted H_β spectrum in Figure 3. The determined widths from the fits are found to be 6.9±0.2 nm and 4.3±0.2 nm for the 0.15 and 0.4 μs time delays, respectively. After applying Equation 3 we see that the N_e are found to be $1.3\pm0.3\times10^{18}$ cm^{-3} and $6.4\pm0.6\times10^{17}$ cm^{-3} for the 0.15 and 0.4 μs time delays, respectively. The line shifts found from Voigt fitting are 0.52±0.2 nm and 0.2±0.2 nm for the 0.15 and 0.4 μs time delays, respectively. The corresponding N_e from Equation 4 are $1.0\pm0.4\times10^{18}$ cm^{-3} and $3.8\pm0.4\times10^{17}$ cm^{-3}, for the early and later measured H_α profiles, respectively. The error margins for the $H_\alpha$red shifts and the corresponding N_e are larger than the line width diagnostic. This is because the line shift is more affected by any signal noise on the H_α line measurement and because of its relatively small size in comparison to the instrument width. The H_α spectra at the 0.15 μs are at N_e greater than 10^{18} cm^{-3} where self-absorption effects may be a concern. A previous effort considered self-absorption of H_α spectra measured from laser-induced plasma measurements made in ambient laboratory air [28]. This work showed that self-absorption effects are not expected to occur for N_e less than 1.5×10^{18} cm^{-3}. In this scope, the N_e found from the H_α line width is not expected to experience a line profile distortion due to self-absorption; however, measurements made at earlier times in the plasma evolution are likely to experience self-absorption and appropriate tests should be performed [30]. One should note that the H_α red shift is likely to experience a minimal impact in the presence of moderate self-absorption, *i.e.* showing no line reversal. The $H_\beta$line is best observed at N_e that are likely not self-absorbed, but it is worth noting that while it is possible for the H_β line shape to become distorted and have its width altered, the peak separation is expected to be independent of self-absorption effects.

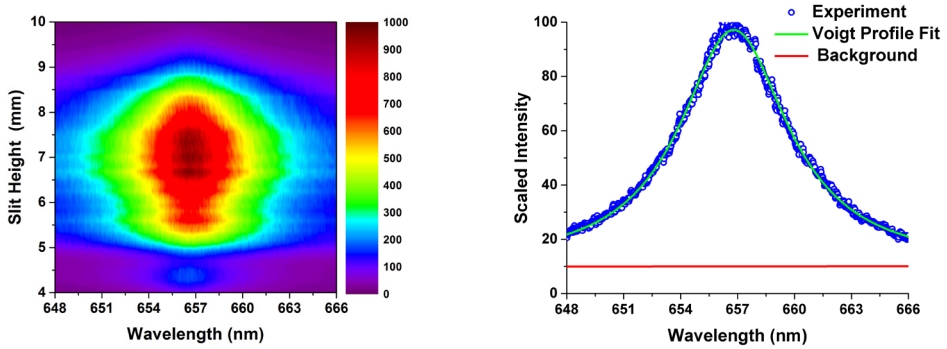

Figure 4: Two dimensional image of H_α spectra at 0.15μs time delay (Left) and Voigt profile fit to an H_α spectrum at a slit height of 6.1 mm used to extract the FWHM (Right)

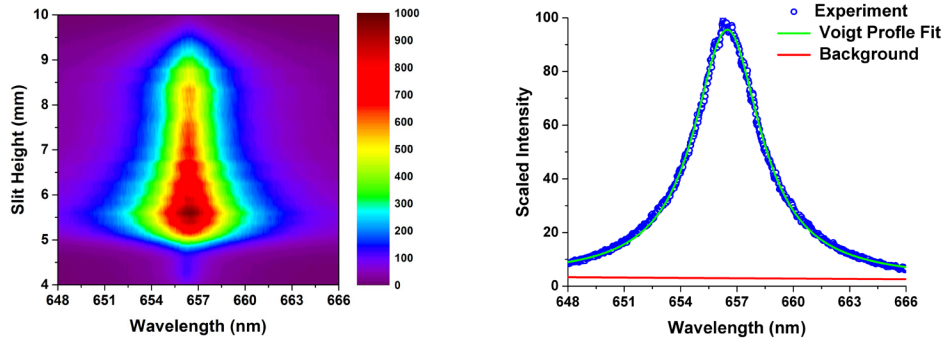

Figure 5: Two dimensional image of H_α spectra at 0.4μs time delay (Left) and Voigt profile fit to an H_α spectrum at a slit height of 6.1 mm used to extract the FWHM (Right)

To serve as a comparison for the N_e determined from the developed empirical formulae, N_e from the H_α and H_β line diagnostics were compared to recent, similar treatments of these line shape N_e diagnostics. The results of this comparison are collected in Table 1. The H_α and H_β line FWHM diagnostics were compared to a recent treatment of fitting methods used to extract the line FWHM and the subsequent empirical formulation that followed [14].The N_e from the peak separation is compared to a recent treatment which is based off of the semi-classical Stark broadening approach and newer computer simulated models [10, 24]. The last column in the table shows N_e found using the experimental data from the current effort, employing formulae from the indicated references. The line width shows remarkable congruence with current empirical formulae, especially under consideration of experimental margins of error. The peak separation is shown to conflict slightly with other methods. This is due to temperature and line width dependencies in the peak separation theory models, as well as considerations of symmetric vs. asymmetric H_β line profiles [24, 25]. For N_e near 1-2×10^{17} cm^{-3} the empirical formula used here is likely suitable and should show congruence with other models. For greater N_e (≥ 3×10^{17} cm^{-3}), the FWHM dependency and asymmetric nature of the H_β line profile become more prominent and exhibit a greater effect on the H_β peak separation diagnostic and a factor of 2 difference between methods is not unexpected. The H_α line width and shift formulae in this work have already been applied to laser ablation of ice surfaces and have been previously presented [23]. This work showed that this formula is a sufficient method for determining the N_e from the H_α line red shift in view of other recent line shift diagnostic methods [9, 15]. As such, the determined values from this work are used to populate the last column of Table 1 for the H_α line red shift diagnostic. Reference [23] showed the line shift was particularly useful for N_e in excess of 10^{18} cm^{-3}.

Table 1
Experimentally determined Balmer series line shape parameters and N_e results of the developed empirical formulae

Diagnostic	*Time Delay (μs)*	*Experimental Value (nm)*	*Empirical Formulae N_e (10^{17} cm^{-3})*	*N_e Reference (10^{17} cm^{-3})*
H_β: Δw	0.65	10.3±0.5	3.2±0.3	3.1±0.3 [14]
H_β: $\Delta\lambda_{ps}$	0.65	3.0±0.6	3.8±0.5	2.1±0.7 [27]
H_α: Δw	0.15	6.9±0.2	13.0±3.0	14.9±4.0 [14]
	0.4	4.3±0.2	6.4±0.6	7.4±0.7 [14]
H_α: Δδ	0.15	0.5±0.2	10.0±4.0	10.0±4.0 [23]
	0.4	0.2±0.2	3.8±0.5	3.8±0.4 [23]

It is important to note that the double peak structure of the H_β line is a part of its measured profile. When comparing to theoretical calculations or simulations of Stark broadened H_β spectra or when fitting with such calculations, one must consider the double peak structure. Previous work has been completed to find an empirical relation for the H_β line width and peak separation from computer simulated Stark broadened hydrogen Balmer series spectra [14, 24], using the tabulated profiles of Gigosos *et al.* [11]. This effort showed that fitting a single Lorentzian profile to the double peak H_β was a sufficient method for extracting the FWHM, which is not the same as fitting with a tabulated profile. Attempts at a double peak fitting method in which the H_β double peak structure is fit with a convolution of two Voigt or Lorentzian profiles have also been completed [19]. This effort is a difficult task given that the central dip of the line becomes filled due to the significant overlap between the two line profiles used in the fit. While the overall goodness of fit may be increased by double peak fitting of this nature to a measured H_β profile, the profile is a single line and is physically represented by a Holtsmark profile; thus, work of this type may quickly develop into a «red herring» of sorts due to its difficulty and non-physical nature, and other pathways to improved fitting to experimental Balmer series line profiles should be considered.

One such pathway may be the consideration of the so-called Holtsmark profile. Though we have followed the customary notion of fitting with a Voigt or Lorentzian line profile to determine the line width from measurements of hydrogen Balmer series lines to find the Stark broadened line component, the actual line profile under Stark boradening for charged plasma perturbers shows a Holtsmark profile [31]. Each type of pertruber (dipoles, quadrupoles, ions, *etc.*) has its own distribution and the profile is taken to be the sum over all these perturbing distributions. The Holtsmark profile itself has Gaussian and Lorentzian characteristics in the line center and wings, respectively. Recent work has also shown it possible to consider convolutions of Lorentzian, Gaussian, and Holtsmark profiles [32].Fitting with and use of this type of profile has the advantage of improved consideration near the line center and far into the line wings, which would lead to improved line shift and ion temperature determinations.

5. SUMMARY

In this work, we have considered the use of the hydrogen Balmer series alpha and beta lines for diagnostics of the high density plasma produced following laser ablation of an aluminum target sample. Empirical formulae that relate the H_α Stark width and shift and the H_β width and peak separation were developed from precisely and previously collected H_α and H_β spectra from laser-induced plasma experiments. The formulae were applied to find the electron density from the current ablation experiments. The H_α N_e from the line widths is found to be $1.3\pm0.3\times10^{18}$ and $6.4\pm0.6\times10^{17}$ cm^{-3} for 0.15 and 0.4 μs plasma delays, respectively. The H_α line shifts indicate N_e values of $1.0\pm0.3\times10^{18}$ and $3.8\pm0.5\times10^{17}$ cm^{-3} for the 0.15 and 0.4 μs time delays, respectively. At a time delay of 0.65 μs, measured H_β line profiles were used to infer N_e values of 3.2 ± 0.3 and $3.8\pm0.5\times10^{17}$ cm^{-3}.

The inferred N_e from the two $H_\beta$diagnosticsindicate close agreement of the electron density inferences. Further, good agreement for the H_α and H_β line width diagnostics with currently existing formulae is found, particularly within the consideration of experimental errors. When considered with the error prone nature of determining the line shifts, decent agreement is found between the H_α line width and line shift diagnostics developed in this work. The H_β peak separation method developed is useful for N_e near $1\text{-}2\times10^{17}$ cm^{-3}. Slight differences occur when the H_β peak separation N_e diagnostic is considered in comparison to other available methods for N_e greater than 3×10^{17} cm^{-3} and factor of 2 differences are not unexpected. Such differences arise due to temperature and line width dependencies on the peak separation model and due in part to considerations of symmetric vs. asymmetric H_β line profiles.

The H_α and H_β line widths and the H_α line shift were extracted from the measured line profiles by fitting with a Voigt profile which had a Gaussian component equivalent to the instrument function. This is a customary practice within the field of experimental laser-induced plasma spectral diagnostics. Future work and application of the determined line shape formulae should focus on improved methods of extracting the line width and line shift parameters of a spectral line. This may be done under the consideration of deconvolutions which include Holtsmark, Gaussian, and Lorentzian broadening components of the spectral line profile.

Acknowledgements

This work is supported by the Center for Laser Applications at the University of Tennessee Space Institute.

References

[1] D.M. Surmick and C.G. Parigger, *J.Phys. B: Atom. Mol. Opt. Phys.*, **48**, (2015), 115701.

[2] A.K. Rai, F. Yueh, and J.P. Singh, *Appl. Opt.*, **42**, (2003), 2078.

[3] M. Sasabi and P. Cielo, *Appl. Spectrosc.,* **44**, (1995), 3654.

[4] A. Mendys, M. Kański, A. Farah-Sougueh, S. Pellerin, B. Pokrywka, and K. Dzierzęga, *Spectrochim. Act.B*, **96**, (2014), 61.

[5] C.G. Parigger, A.C. Woods, D.M. Surmick, L.D. Swafford, and M.J. Witte, *Spectrochim. Act. B*, **99**, (2014), 14.

[6] H.J. Kunze, *Introduction to Plasma Spectroscopy*, Springer Verlag, Berlin, (2009).

[7] D.A. Cremers and L.J. Radziemski, *Handbook of Laser-Induced Breakdown Spectroscopy*, John Wiley and Sons, Hoboken, NJ, (2006).

[8] C.G. Parigger, *Spectrochim. Act. B*, **79**, (2013), 4.

[9] H.R. Greim, J. Halenka, and W. Olchawa, *J. Phys. B: Atom. Mol. Opt. Phys.*, **38**, (2005), 975.

[10] C.R. Vidal, J. Cooper, and E.W. Smith, *Astrophys. J. Suppl. Ser.*, **25**, (1973), 37.

[11] M.A. Gigosos, M.A. González, V. Cardeñoso, *Spectrochim. Act. B*, **58**, (2003), 1489.

[12] M. A. Gigosos and V. Cardeñoso, *J. Phys. B: Atom. Mol. Opt. Phys.*, **29**, (1996), 4795.

[13] H.R. Griem, *Spectral Line Broadening by Plasmas*, Academic Press, New York, (1974).

[14] N. Konjević, M. Ivković, and N. Sakan, *Spectrochim. Act. B*, **76**, (2012), 16.

[15] J.F. Kielkopf and N.F. Allard, *J. Phys. B: Atom. Mol. Opt. Phys.*, **47**, (2014), 155701.

[16] E. Oks, *Stark Broadening of Hydrogen and Hydrogenline Spectral Lines in Plamas: The Physical Insight*, Alpha Science International, Oxford, (2006).

[17] A. Escarguel, E. Oks, J. Richou, and Volodko, *Phys. Rev. E*, **62**, (2000), 2667.

[18] Y. Ispolatov and E. Oks, *J. Quant. Spectrosc. Radiat. Transf.*, **51**, (1994), 129.

[19] C.G. Parigger, L.D. Swafford, A.C. Woods, D.M. Surmick, M.J. Witte, *Spectrochim. Act.*, **99**, (2014), 28.

[20] H.R. Griem, *Plasma Spectroscopy*, McGraw-Hill, New York, (1964).

[21] H.R. Girem, *Principles of Plasma Spectroscopy*, Cambridge University Press, New York, (1997).

[22] C.G. Parigger, D.H. Plemmons, and E. Oks, *Appl. Opt.*, **42**, (2003), 5992.

[23] C.G. Parigger, D.M. Surmick, G.Gautam, and A.M. el Sherbini, *Opt. Lett*, **40**, (2015), 3346.

[24] M. Ivković, N. Konjević, and Z. Pavlović, *J. Quant. Spectrosc. Radiat. Transf.*, **154**, (2015), 1.

[25] G. Gautam, D.M. Surmick, and C.G. Parigger, *J. Quant. Spectrosc. Radiat. Transf.*, **160**, (2015), 19.

[26] C.G. Parigger, A.C. Woods, M.J. Witte, L.D. Swafford, and D.M. Surmick, *J. Vis. Exp.*, **84**, (2014), E51250.

[27] W. Sdorra and K. Niemax, *Mikrochim. Act.*, **107**, (1992), 319.

[28] C.G. Parigger, L.D. Swafford, D.M. Surmick, M.J. Witte, A.C. Woods, and G. Gautam, *J. Phys.: Conf. Ser.*, **548**, (2014), 012043.

[29] M.F. Zaghloul, *ACM Math. Software*, **38**, (2011), 15:1.

[30] H. Moon, K.K. Herrera, N. Omenetto, B.W. Smith, and J.D. Winefordner, *Spectrochim. Act. B*, **64**, (2009), 702.

[31] J.P. Holtsmark, *Annalen der Physik (adp)*, **338**, (1919), 577.

[32] A. Sapar, R. Poolamae, and L. Sapar, *Baltic Astronomy*, **15**, (2006), 435.